RZ 3272 (# 93318) 08/21/00
Mathematics & Physics 17 pages

Research Report

STM-Excited Electroluminescence and Spectroscopy on Organic Materials for Display Applications

S.F. Alvarado*, L. Rossi, P. Müller, P. F. Seidler, and W. Rieß

IBM Research
Zurich Research Laboratory
8803 Rüschlikon
Switzerland

STM-Excited Electroluminescence and Spectroscopy on Organic Materials for Display Applications

S.F. Alvarado†, L. Rossi, P. Müller, P. F. Seidler, and W. Rieß

IBM Research, Zurich Research Laboratory, 8803 Rüschlikon, Switzerland

Abstract

Presented here is an overview of the current status of our work on scanning-tunneling-microscope-based (STM) spectroscopy and electroluminescence (EL) excitation to study the physical and electronic structure of organic materials used in organic light-emitting devices (OLEDs). By these means we probe the critical device parameters in charge-carrier injection and transport, i.e. the height of the barrier for charge-carrier injection at interfaces between different materials and the energy gap between positive and negative polaronic states. In combination with optical absorption measurements, we gauge the exciton binding energy, a parameter that determines energy transport and electroluminescence efficiency. In STM experiments involving organic electroluminescence excitation the tip functions as an OLED electrode in a highly localized fashion, allowing one to map the spatial distribution of the EL intensity across thin-film samples with nanometer lateral resolution as well as to measure the local EL emission spectra and the influence of thin-film morphology.

I. INTRODUCTION

Since the recent development of high-efficiency organic light-emitting devices (OLEDs), many experimental and theoretical investigations have been undertaken to elucidate the underlying fundamental physical processes. Knowledge of the relative alignment of the energy levels at interfaces between organic materials is crucial in order to understand the device operation and, in particular, the physics of charge-carrier injection, transport, and radiative recombination, with the ultimate goal of improving electroluminescence efficiency. The alignment of the highest occupied molecular orbitals (HOMOs) at the interfaces of an OLED is usually estimated from the ionization potential (IP) of each material by using the Schottky-Mott rule [1], which assumes that the energy levels correspond to a common vacuum level (CVL), thus neglecting surface, interface and charge-transfer effects. The alignment of the lowest unoccupied molecular orbital (LUMO) is determined by adding the band gap, measured from optical absorption, to the HOMO energy, a procedure that neglects the exciton binding energy as well as molecular levels of optically forbidden electronic transitions. This method for modeling OLED energy diagrams is a useful first approximation, but can lead to significant errors. For instance, studies carried out using techniques such as ultraviolet photoemission spectroscopy (UPS), [2–7], internal photoemission [8,9], and scanning tunneling microscope (STM) spectroscopy [10–12] show clear evidence of significant deviations from the CVL rule for organic/metal as well as for organic/organic interfaces. In addition, experimental studies show that the actual gap for charge-carrier injection into organic materials can be significantly larger than the optical band gap [8,12]. The excess energy is due to the binding energy of the singlet exciton, $E_{\rm b}$. For example for the commonly used material poly(*p*-phenylenevinylene) (PPV) and its derivatives, $E_{\rm b}$ has been determined by a number of different techniques, and values between 200 and 500 meV have been obtained [8,12–16]. Other measurements, however, have suggested values as low as 25 meV [17] or as high as 1 eV [18,19]. Those experimental results in turn beg the question: What are the physical and chemical phenomena that determine the energy-level alignment and transport properties for organic-organic and organic-metal interfaces?

In this report we show how STM-based techniques can be employed to probe the electronic and transport properties of organic materials, which can lead to new attempts to answer the above question. In fact, one important capability of the new STM-based techniques described here is that they allow one to take direct measurements of the molecular level alignment of the filled as well as of the empty states of all the interfaces of a multilayer OLED. A technique that allows the alignment of the empty states to be determined in a direct way is particularly welcome because photoemission spectroscopy techniques have so far proved useful only to probe the occupied levels of organic materials. Here we discuss results obtained with thin films of organic materials used in the prototypical Kodak OLED structure consisting of a vapor-deposited stack of copper phthalocyanine (CuPc), N,N'-di(naphthalen-1-yl)-N,N'-diphenyl-benzidine (NPB), and *tris*(8-hydroxyquinolato)aluminum (Alq_3) thin-film layers [20]. Each of the organic layers in the OLED fulfills a specific function. The electroluminescent layer is Alq_3, a highly efficient fluorescent material that predominantly transports electrons, whereas NPB is a good hole-conducting material. CuPc is a buffer layer inserted between the anode and the NPB layer to improve device stability [20,21]. Crucial to the performance of the device is the relative alignment of the energy levels of each of its components. Of particular interest is the Alq_3/NPB interface, where the energy levels form a potential barrier that confines electrons on the Alq_3 side and holes on the NPB side, i.e. an accumulation region is formed

that promotes radiative recombination [22].

II. CHARGE-CARRIER INJECTION FROM THE STM TIP INTO ORGANIC MATERIALS

A basic condition in scanning tunneling microscopy and spectroscopy is that the tunneling resistance $R_{\rm T} = V_{\rm T}/i_{\rm T}$ has to be much higher than the resistive losses associated with current flow through the sample (spreading resistance). The charge injection process takes place by means of tunneling through a vacuum potential barrier, see Figure 1. Since the applied bias voltage, $V_{\rm T}$, is dropped at the tunneling barrier, the charge-carrier injection energy can be tuned through the polarity and magnitude of $V_{\rm T}$. This is the model underlying the spectroscopy technique for the determination of the density of states in the *surface region* by means of i-V curves collected with the STM-feedback loop disconnected [23]. If the resistive losses within the organic material are allowed to become comparable to $R_{\rm T}$, however, the surfaces of the tip and the sample can come into close proximity and make physical contact, causing the vacuum barrier to collapse. In the following we discuss charge-carrier injection as well as the electric-field distribution for this particular case. In the subsequent sections we discuss how this injection mode can be used to probe locally the transport properties of soft organic materials as well as electronic excitations and molecular energy levels at organic interfaces.

We begin by noting that when the tip makes contact with the organic surface its Fermi level is pinned, typically at an energy within the energy gap. This gives rise to the formation of a Schottky barrier, and the bias voltage drops fully within the organic material. Figure 2 shows the geometry and energy diagrams for negative tip polarity (tip negative, $V_{\rm T} < 0$, relative to the anode's Fermi level) and for a magnitude of $V_{\rm T}$ such that the Fermi level of the tip is above the threshold for injection into the lowest electron polaron state of the organic material. Here the average field at the injection spot is $E_m = (V_{\rm T} - V_{\rm bi})/d$, where $V_{\rm bi}$ is the tip/substrate contact potential and d the distance between the tip apex and the substrate when the tip is in contact with the organic material. The energy diagram corresponds to that of a single-layer OLED, but with one significant difference: the strength of the electric field is much higher at the apex of a tip than at a planar electrode interface. In this configuration injection of charge carriers takes place by tunneling through the Schottky barrier into polaron states of the organic material [24]. (Charge injection from Schottky barriers into organic material has been the topic of several theoretical studies, see for instance Refs. [24,25]).

In the spherical apex approximation, the electric field near a tip apex of effective radius R drops off as $1/(R+r)^n$, with distance r from the tip, where $n = 2$ for the case of ohmic and $n = 1/2$ for space-charge-limited (SCL) current flow [26]. This field distribution, characterized by an enhanced electric field at the tip apex, the radius of which is typically a few to several tens of nanometers, is the reason why it is possible to inject extremely high current densities in STM experiments. These current densities are estimated to be in the range of $j = 10$ - 10^4 A/cm^2, orders of magnitude higher than those used in standard planar-contact OLED devices, where typically $j < 1$ A/cm^2. The ratio between the field at the apex and the field at the substrate, $E_{\rm T}$ and $E_{\rm S}$, is approximately [27]

$$E_{\rm T}/E_{\rm S} \cong [(\kappa R + d)/\kappa R]^n \ , \tag{1}$$

where κ is a modifying factor to account for the geometry of the real system. For instance $\kappa > 1$ for $R \ll d$ due to the effect of the tip's shaft, whereas $\kappa < 1$ for $R \cong d$ due to the proximity

of the planar substrate [27]. Note that the actual injection process can be either thermionic emission or tunneling [28], depending on the barrier heights, field strengths at the injection interface (which depends on the actual sharpness of the tip), and temperature. For barrier heights of approximately 1 eV and average fields in the neighborhood of 0.1–1 V/nm, typical values in the experiments described below, we expect predominantly tunneling injection [28], whereas for barrier heights well below 1 eV thermionic emission might become significant.

The question arises as to what is the current balance for the point-contact injection geometry compared to the planar OLED case. The electric field is significantly higher at the tip apex than at the substrate interface, which translates, exponentially, into a much higher injection probability of charge carriers across the corresponding Schottky barrier from the tip than from the substrate. Consequently, the current passing through the tip/organic-material/substrate system is expected to be predominantly monopolar. There are, however, some requirements for this to hold, such as that R is small and that the barrier height for oppositely charged carrier injection from the substrate is not much smaller than the barrier height at the tip [27].

Regarding tip penetration it is clear that if the magnitude of V_{T} is decreased while keeping i_{T} constant, the feedback loop causes the tip to move into the sample, decreasing d to counterbalance the decrease in R_{T}. Here the requirement is that the tip motion compensates for the electric field reduction associated with the change in V_{T} to maintain constant tunneling current flow across the barrier. Note that as the tip contact area increases with decreasing d, the electric field required for injection and transport is somewhat lowered as the tip moves into the sample. This electric field reduction is relatively small, however, because of the exponential dependence of the injection probability on the electric field. In addition, as the electric field is strongest at the tip apex and decreases with injection angle, Θ, the thickness (D_{B}) is thinnest for tunneling in the $\Theta = 0$ direction. This implies that the *effective injection* area does not change strongly with d, except in the initial stages of contact, $d \cong D$, where D is the thickness of the thin film (see Figure 2).

III. MEASUREMENT OF THE BARRIER HEIGHT FOR CHARGE-CARRIER INJECTION

The measurement of z–V curves can be used as a spectroscopy technique to probe the density of states of the material in a manner that differs from the standard i–V spectroscopy technique. More specifically, as the magnitude of the bias voltage is decreased, the tip penetrates the organic material and can inject charge carriers in the neighborhood of the substrate interface, see Figure 2b. Obviously charge-carrier injection into the organic material is possible until, at a characteristic threshold voltage at which the Fermi level of the tip moves into the forbidden energy gap *at the interface with the substrate*, the tip penetrates deeply into the organic material, reaching the interface region where charge carriers can be injected into the substrate either by directly tunneling into it or via nonresonant tunneling through molecules in contact with it. This threshold voltage (V_{th}), typically identified by a sharp decrease in the slope (dz/dV) of the z–V curve, marks the threshold for injection into the lowest electron polaron state for negative tip polarity, and is thus a measure of the potential barrier for electron injection at the *buried interface of the organic material*, see Figure 2b. Repeating this gedanken experiment for positive tip polarity we can convince ourselves that the barrier for hole injection into polaronic states can be measured using the same procedure. We emphasize that the z–V technique works only for soft materials that yield to the pressure exerted by the

tip [29].

Figure 3 shows z–V spectra collected on Alq_3 thin films deposited on a Au(111) surface. The typical z–V tip displacement for a clean Au(111) is shown as a dashed line. The measurements on Alq_3 thin films yield a threshold energy of $E_{P^-} = 1.15 \pm 0.180$ eV for electron injection, and $E_{P^+} = -1.81 \pm 0.25$ eV for hole injection, relative to the Fermi level of the Au(111) substrate. From these results we can directly determine the band gap for injection of charge carriers into polaron states, the so-called single-particle energy gap [8]. Note that this is the energy gap that one should use to model the energy diagram of OLEDs. Figures 4a and 4b show histograms of the electron injection threshold of Alq_3 thin films deposited on Au(111) and Ag(111) substrates. Each event represents a threshold measurement taken on a different spot of the sample. Clearly the distribution reveals the existence of regions where the injection threshold for electrons is 0.6 to 0.7 eV higher. In these regions the energy gap appears to be slightly larger, by approximately 80 meV (average). A possible cause for this shift is the occurrence of various Alq_3 morphologies [30] or shape isomer domains, which can have different interactions with the substrate. In Section VI we discuss STM-excited spectroscopy measurements that provide further evidence for this interpretation. We note that local variations of the substrate properties, due to contaminants for instance, can also induce a shift of the energy levels of the molecular orbitals. However, as the measurements were performed on samples grown in ultrahigh vacuum conditions, the latter explanation seems implausible.

In the following we compare the values of the barrier heights determined by z–V spectroscopy with the predictions of the CVL approximation, bearing in mind that, given the uncertainties of our measurements and those of others, only differences of more than 0.3–0.4 eV are significant. The scatter of the IP values for organic materials reported by different groups is of this magnitude. Despite these relatively important shifts of the injection threshold we find that the energy levels of Alq_3 clearly align below the CVL estimate for the Au(111) substrate where a barrier height for electron injection of 2–2.5 eV is estimated from the ionization potentials of 5.31 eV for Au(111), [31] and 5.57–6.0 eV for Alq_3, [2,3,32–36] and the single particle band gap of 2.96±0.13 eV, see below. In addition, we see that the electron injection barrier is approximately 200 meV higher on Au(111) than on Ag(111). The magnitude of the shift is, however, smaller than the value of approximately 600 meV calculated by taking the difference between the work function of the Ag(111) (4.74 eV [31]) and the Au(111) surfaces. These deviations from the simple CVL model indicate the effect of image forces or the formation of a dipole layer at the surface, due to negative charge transfer from Alq_3 to the metal substrate. A similar result for hole injection also shows the invalidity of the CVL model, and our values for the threshold of the occupied states, see above, confirm the results of UPS measurements on the Alq_3/Au(111) system [2–4].

IV. PROBING THE EXCITON BINDING ENERGY

The combination of a hole polaron and an electron polaron (P^+, P^-, respectively) results in the formation of an exciton. The exciton binding energy has been defined [37] as $E_b = E_{gsp} - E_a$, where E_{gsp}, the difference between the electron and hole polaron energies, is called the single-particle energy gap [8] and E_a is the energy required to create a molecular exciton as determined from optical absorption spectra (the diagram in Figure 5 illustrates this definition). Here HOMO and LUMO represent the one-electron band picture, which neglects Coulomb

and exchange interactions as well as molecular relaxation effects. Supplying the exciton with energy E_b gives rise to the creation of a pair of oppositely charged polarons. In an organic material the radiative decay of a singlet exciton results in the emission of a photon. From a series of z–V measurements as well as from electroluminescence intensity vs. V_T measurements (described below) we find that $E_{gsp} = 2.96 \pm 0.13$ eV for Alq_3. Combining this result with the threshold for optical absorption of Alq_3, $E_a \cong 2.75$ eV, we obtain $E_b = 220 \pm 130$ meV. This result compares well with the theoretical results of *ab initio* calculations by Andreoni and Curioni [38]. Note that the polaron self-trapping energy is expected to be different for the facial and the meridianal isomers [39].

Figure 6 shows z–V measurements performed on a thin film of NPB deposited on an InN substrate. For this material we find $E_{gsp} = 3.30 \pm 0.16$ eV. The optical absorption gap of this material is $E_a = 3.0$ eV [40,41], from which we obtain $E_b = 300 \pm 160$ meV. The results for CuPc single layers [42] indicate that the gap for charge-carrier injection is *smaller* than the optical gap, $E_a = 1.6$ - 1.7 eV (see next section) [43]. This fact is evidence that the injection and transport involve molecular orbital states not accessible by optical means [42].

V. STM AS A PROBE OF LOCAL CONDUCTIVITY

The rate of penetration, dz/dV, deserves some attention because it depends on local charge-carrier transport characteristics of the material, as shown in the following. We begin by considering the voltage bias, V_c, at which the tunneling barrier collapses, noting that this point is marked by an increase of the slope of z–V because of the onset of penetration. For a given constant i_T and hypothetical thin films of equal thickness D it is easy to see that in order to sustain the current flow through the injection region a lower electric field is required for high conductance than for low-conductance materials. In other words, $D/|V_{ch} - V_{th}| > D/|V_{cl} - V_{th}|$, where V_{ch} and V_{cl} denote the voltages at which the tunneling barrier collapses for high and low-conductance materials, respectively. Thus in contact mode we expect the average slope of the z–V curves to be directly proportional to the conductivity of the sample. This implies that, in point-contact mode, the z–V curves can yield information about the transport properties of organic materials. From the above considerations we can additionally conclude that, for a given sample conductance, the rate of penetration is proportional to the tunnel resistance, i.e., inversely proportional to i_T, a fact that we have verified experimentally [42].

In the following we compare z–V measurements performed on organic materials with very different transport properties, namely the hole conductors CuPc and NPB, and the electron conductor Alq_3. We also show how relative electron and hole mobilities can be probed by means of this technique. Figure 7a displays a typical z–V curve collected on a CuPc thin film deposited on a Au(111) substrate. Figure 7b depicts the surface crystal structure of one of the polymorphic crystallites on which the curve was collected [42]. For these measurements the bias voltage was ramped with decreasing magnitude for each polarity. Each z–V run begins with the tip biased at a potential difference high enough to ensure that the tip is above the surface of the organic film to avoid modifying or damaging the organic thin-film structure before the actual collection of data. Typical z–V curves for a clean Au(111) substrate are shown as dashed lines. The height difference between the two curves in the high-voltage region is an approximate measure of the local thickness of the organic thin film. At high bias voltages the molecules at the free surface of the thin film can be clearly imaged (see Figure 7b). As the bias voltage is decreased we observe that the tip moves into the thin film in a step-like

fashion, initially by only one or two molecular spacings. In some cases the z–V curves exhibit several step-like transitions before full penetration (see Figure 7a). A striking feature of the z–V curves is the steepness of the curves near threshold, $dz/dV \cong 2 \times 10^2$ nm/V. Actually the z–V curves collected on CuPc resemble the ideal step function expected for a highly conducting material with a band gap: in the high-voltage range the tip follows approximately the shallow z–V displacement typical of a clean metallic surface until, suddenly, it penetrates the organic material when its Fermi level shifts to energies very close to the forbidden gap.

In comparison z–V curves collected on Alq_3 or NPB thin films exhibit a much shallower slope, typically 1.4 - 3 nm/V, see Figures 3 and 6. As discussed above these results indicate that the conductivity of CuPc is much higher than that of Alq_3. This is indeed the case: the mobility of the majority charge carriers of CuPc, μ_h, is in the realm of 10^{-3} cm^2 V^{-1} s^{-1} (cf. e.g. Ref. [44]), whereas that of Alq_3 [45,46] is $\mu_e \leq 10^{-4}$ cm^2 V^{-1} s^{-1} at high electric fields. Note, additionally, that the slope of the z–V curve for Alq_3 is steeper for electron than for hole injection, indicating that the resistivity for electron transport is lower than for hole transport. This is in agreement with experimental results showing that the electron mobility is about two orders of magnitude higher, than the hole mobility in this material (cf. e.g. [46]). On the other hand, measurements on the hole conductor NPB, shown in Figure 6, show the reverse trend, namely that the slope of the z–V curve is steeper for hole than for electron injection, as we would expect when the hole mobility is greater than the electron mobility.

The above experimental results show that the z–V curves can be used to characterize the transport properties of organic materials. For a more quantitative interpretation of the results, however, one has to take into account that the slope of the z–V curve can be influenced by various factors, for instance: (a) the actual height and thickness of the injection barrier, the latter of which is also sensitive to the sharpness of the tip; and (b) the relatively strong field dependence of the charge-carrier mobility typical of amorphous organic materials with low mobility. Finally we note that the actual value of the slope of the z–V curves is found to depend on the particular spot on which the curve is taken, showing that there are quantifiable in-plane variations of the transport properties of the thin film.

VI. ELECTROLUMINESCENCE GENERATION BY CHARGE-CARRIER INJECTION FROM THE STM TIP

The possibility of using an STM to generate electroluminescence (EL) with nanometer spatial resolution and in this way to probe the electronic properties of organic materials has been demonstrated in experiments on various materials [10,11,47–50]. In STM-excited luminescence (STL) on organic materials, charge carriers from the tip tunnel into polaron states and, by combining with carriers of opposite polarity injected from the substrate, excitons are formed that can decay radiatively. Four kinds of STL experiments have been performed: (1) Simultaneous collection of topography and wavelength-integrated EL intensity (I_L) maps; (2) measurements of I_L vs. V_T curves; (3) EL spectroscopy, in which wavelength-resolved spectra are collected at different spots of the sample; and (4) EL intensity decay with time for charge-carrier injection at a fixed point of the sample. The experimental setup is shown schematically in Figure 8 (see the references for experimental details [11]).

We begin by briefly discussing the surface morphology of the Alq_3 thin films deposited on Au(111) substrates and its effect on the spectral distribution of the EL. The STM images reveal that the surface of thin films of Alq_3 exhibit different morphological features even on

the same sample and within regions separated by less than 1 μm. As an example, images collected on neighboring spots of a thin film approximately 5-nm thick are shown in Figure 9. The surface region shown in Figure 9a exhibits flat domains with a roughness of 0.11 nm (rms) where terraces can be identified. In some cases these domains exhibit parallelepiped-like features approximately 10 nm wide and 100 nm long. The heights of these features as well as that of the terraces seems to be defined by molecular layers of thicknesses that vary at different spots of the sample in the range from 0.52 to 0.7 nm, indicating different molecular packing habits [30]. On other regions of the samples, however, no terraces can be identified and the surface corrugation is significantly higher, see Figure 9b. The formation of flat molecular domains and terraces seems to be favored in thinner films. For instance for a film of thickness $D \cong 2.5$ nm, we found regions of the organic layer so uniform and smooth that the atomically flat terraces of the underlying Au(111) substrate, in some cases even its herringbone surface reconstruction [51], are mimicked on their surface. Still, we found no clear evidence of in-plane crystalline order at the molecular level in our samples, a result showing that the thin films do not have a strong tendency to crystallize but, rather, that they are probably disordered or amorphous in the plane of the terraces. Conversely for films much thicker than 5 to 7 nm, where the absolute surface corrugation is higher, we did not find smooth flat terraces.

STM-excited electroluminescence spectra collected on smooth and rough regions, show clear differences (see Figure 10): the film regions characterized by smoother surfaces exhibit spectra with a distinct and narrow dominant peak at $h\nu = 1.8 \pm 0.03$ eV, and a weaker peak at $h\nu = 1.98 \pm 0.03$ eV, both having a line width of $\simeq$100 meV (FWHM), whereas on the regions with rougher surface morphology the intensity of the second peak is much higher [10]. Actually the spectra appear as if they arise from a linear superposition of spectra from two different kinds, e.g. polymorphic forms or shape isomers, of Alq_3. As discussed in the section on barrier height determination above, this is also a possible explanation for the double distribution of injection thresholds found in the z–V curves of this material. We note that the spectra are red-shifted with respect to the emission from Alq_3 in OLED devices, which normally peaks at about 2.3 eV (cf. e.g. [40]). This shift appears to be induced by the intrinsic fluorescence of the tip-Au(111) tunneling junction [10], which arises from the enhanced radiative decay of collective excitations, i.e. plasmons, involving the tip and the metallic surface [52]. This shows that collective excitations (plasmons) involving the tip and the substrate can play an important role in the excitation of light emission, particularly for very thin organic films. Measurements show that the luminescence efficiency increases with the organic thin-film thickness, which suggests quenching of the Alq_3 emission due to the proximity of the metal surface.

Figure 11 shows an EL intensity, I_{L}, versus V_{T} curve collected on an Alq_3 thin film deposited on Au(111). The curve is the average of several $I_{\mathrm{L}} - V$ curves collected on different spots of the sample. Owing to statistical noise the error in the EL threshold determination is somewhat higher than that for the injection threshold determined from z–V curves. Nevertheless the energy difference between the EL thresholds of light emission for each of the charge carriers agrees reasonably well with the z–V spectroscopy results. Typically we find that the slope of the I_{L} vs. V_{T} curves is approximately twice as high for positive than for negative tip polarity. This higher EL efficiency for positive tip polarity is an indication of a different charge-carrier balance for different tip polarities: for positive tip polarity, hole (minority charge carrier) injection into the organic material is more efficient than for negative tip polarity, i.e., the ratio of the hole and electron currents, $i_{\mathrm{h}}/i_{\mathrm{e}}$, is higher for positive tips, thus giving rise to an increase of radiative recombination events within the organic material.

Finally, it is interesting to consider STL as a technique for degradation studies of organic

materials. Regarding the tip/organic material/substrate system as a model OLED, our typical experimental parameters correspond to current densities in the range of 10 to 10^4 A/cm^2 for bias voltages well below 10 V. Such enormous current densities, which would normally be considered unreasonable in conventional OLEDs at such low voltages, are attainable because of the extremely high fields at the apex of the STM tip. Thus the STM can be used to perform accelerated aging experiments at current density levels not attainable in a standard planar OLED. Conventional OLEDs often show a decrease of the EL intensity, which depends on the amount of charge having passed through the device. In one study [53], the dependence of the time to half brightness was found to have the form $\tau_{1/2} \propto j^{-x}$, where $1.5 \leq x \leq 1.8$. From this expression we can extrapolate to obtain the half time of an OLED operated at the typical device current densities of 1 - 10 mA/cm^2. For example from measurements performed in ultra-high vacuum conditions on the conjugated polymer PPV operating at an estimated current density of $j \cong 2$ kA/cm^2 and a voltage of $V_{\mathrm{T}} \cong 4.6$ V, the time to half brightness is several hours [11]. From the above expression we extrapolate that for an OLED device operated at 10 mA/cm^2, the half lifetime would exceed tens of thousands of hours even for the typically claimed Coulomb aging case where $x = 1$. Preliminary results for Alq_3 show similar decay behavior, indicating that some organic materials are sufficiently stable that they are not the limiting factor in obtaining the lifetimes of tens of thousands of hours required for device applications, e.g. for emissive displays.

VII. CONCLUDING REMARKS

STM-based tip-contact techniques have been presented that allow the local electronic and transport properties of organic materials to be probed. STM imaging is used primarily to select and define the location of the experiment. It is then possible to probe (a) the barrier heights for injection of positive and negative charge carriers across interfaces, (b) the energy gap for single charge carrier injection, (c) the exciton binding energy, and (d) charge-carrier transport properties such as the qualitative differences between electron and hole mobilities. In addition, STL measurements have been used to study the local electronic excitations of thin organic layers. For the case of Alq_3, for example, we find that the spectral features of the luminescence depend on the structural details of the film, possibly indicating the effects of different polymorphic and/or isomeric forms.

The STL and z–V spectroscopy techniques complement and far exceed the capabilities of photoelectron emission spectroscopy (PES), the standard technique used to study the energy level alignment at interfaces, which can probe only the HOMO levels and has limited spatial resolution.

ACKNOWLEDGMENTS

Many thanks to R. Schlittler for technical assistance, T. Beierlein for growing the NPB layers, R. Beyeler for help characterizing the thin-film samples, E. Delamarche and A. Bietsch for preparing gold and silver substrates, A. Curioni, W. Andreoni, M. Kemerink, and H.W.M. Salemink for many interesting and enlightening discussions. Thanks also to H. Riel for providing the optical absorption measurements on Alq_3, NPB and CuPc thin films.

[1] W. Schottky, *Z. Physik* **118**, 539 (1942); see also W.Mönch, *Surf. Sci.* **132**, 92 (1983).
[2] K. Sugiyama, D. Yoshimura, T. Miyamae, T. Miyazaki, H. Ishii, Y. Ouchi, and K. Seki, *J. Appl. Phys.* **83**, 4928 (1998); H. Ishii and K. Seki, *IEEE Trans. Electron Dev.* **44**, 1295 (1997); K. Seki, E. Ito, and I. Ishii, *Synthetic Metals* **91**, 137 (1997).
[3] A. Rajagopal, C. I. Wu, and A. Kahn, *J. Appl. Phys.* **83**, 2649 (1998); I. G. Hill, A. Rajagopal, A. Kahn, and Y. Hu, *Appl. Phys. Lett.* **73**, 662 (1998).
[4] S. T. Lee, X. Y. Hou, M. G. Mason, and C. W. Tang, *Appl. Phys. Lett.* **72**, 1593 (1998).
[5] T. Mori, H. Fujikawa, S. Tokito, and Y. Taga, *Appl. Phys. Lett.* **73**, 2763 (1998).
[6] R. Schlaf, B. A. Parkinson, P. A. Lee, K. W. Nebesny, and A. R. Armstrong, *J. Phys. Chem. B* **103**, 2984 (1999).
[7] S. C. Veenstra, U. Stalmach, V. V. Krasnikov, G. Hadziioannou, H. T. Jonkman, A. Heres, G. Sawatsky, *Appl. Phys. Lett.* **76**, 2253 (2000).
[8] I. H. Campbell, T. W. Hagler, D. L. Smith, and J. P. Ferraris, *Phys. Rev. Lett.* **76**, 1900 (1996).
[9] G. L. J. A. Rikken, Y. A. R. R. Kessener, D. Braun, E. G. J. Staring, and A. Demandt, *Synthetic Metals* **67**, 115 (1994).
[10] S. F. Alvarado, L. Libioulle, and P. F. Seidler, *Synthetic Metals* **91**, 69 (1997).
[11] S. F. Alvarado, W. Rieß, and P. F. Seidler, *Phys. Rev. B* **56**, 1269 (1997).
[12] S. F. Alvarado, P. F. Seidler, D. G. Lidzey, and D. D. C. Bradley, *Phys. Rev. Lett.* **81**, 1082 (1998); L. Rossi, S. F. Alvarado, W. Rieß, S. Schrader, D. G. Lidzey, and D. D. C. Bradley, *Proc. 2nd Int'l Conf. on Electroluminescence of Molecular Materials and Related Phenomena (ICEL-2)* Sheffield, UK, May 13-15, 1999 (to be published in Synthetic Metals).
[13] R. N. Marks, J. J. M. Halls, D. D. C. Bradley, R. H. Friend, and A.B. Holmes, J. Phys. Cond. Mat. **6**, 1379 (1994).
[14] S. Barth, S. Deussen, and H. Bässler, *Phil. Trans. R. Soc. London A* **355**, 749 (1997); S. Barth and H. Bässler, *Phys. Rev. Lett.* **79**, 4445 (1997).
[15] E. L. Frankevich, A. A. Lymarev, I. Sokolik, F. F. Karacz, S. Blumenstengel, R. H. Baughman, and H. H. Hörhold, *Phys. Rev. B* **46**, 9320 (1992).
[16] M. Scheidler, U. Lemmer, R. Kerstin, S. Karg, W. Rieß, B. Cleve, R. F. Mart, H. Kurz, H. Bässler, E. O. Göbel, and P. Thomas, *Phys. Rev. B* **54**, 5536 (1996).
[17] C. H. Lee, G. Yu, D. Moses, and A. J. Heeger, *Phys. Rev. B* **49**, 2396 (1994).
[18] J. M. Leng, S. Jeglinski, X. Wei, R. E. Benner, Z. Vardeny, F. Guo, and S. Mazumdar, Phys. Rev. Lett. **72**, 156 (1994).
[19] M. Chandross, S. Mazumdar, S. Jeglinski, X. Wei, Z. V. Vardeny, E. W. Kwock, and T. M. Miller, *Phys. Rev. B* **50**, 14702 (1994).
[20] S. A. Van Slyke, C. H. Chen, and C. W. Tang, *Appl. Phys. Lett.* **69**, 2160 (1996).
[21] S. A. Van Slyke and C. W. Tang, *U.S. Patent 472,043,2* (1988); C. Adachi, K. Nagai, and N. Tamoto, *Appl. Phys. Lett.* **66**, 2679 (1995).
[22] C. W. Tang and S. A. Van Slyke, *Appl. Phys. Lett.* **51**, 913 (1987); C. W. Tang, S. A. Van Slyke, and C. H. Chen, *J. Appl. Phys.* **65**, 3610 (1989).
[23] See, for example, R. Feenstra, *Phys. Rev. B* **50**, 4561 (1994); C. Julian Chen, "Introduction to Scanning Tunneling Microscopy," *Oxford Series in Optical and Imaging Sciences*, M. Lapp, J-I. Nishizawa, B. B. Snavely, H. Stark, A. C. Tam, and T. Wilson, Eds., Oxford University Press, New York, 1993; R. Wiesendanger, "Scanning Probe Microscopy and Spectroscopy," *Methods and Applications*, Cambridge University Press, 1994.
[24] E. M. Conwell and E. W. Wu, *Appl. Phys. Lett.* **70**, 1867 (1997).
[25] M. N. Bussac, D. Michoud, and L. Zuppiroli, *Phys. Rev. Lett.* **81**, 1678 (1998).
[26] M. A. Lampert and P. Mark, *Current injection in solids*, Academic Press, H. G. Booker and N.

DeClaris, Eds., New York and London, 1970.
[27] S. F. Alvarado, in preparation.
[28] See for instance A. van der Ziel, *Solid State Physical Electronics*, W. L. Everitt, Ed., Prentice Hall, 1968.
[29] The phenomenon of tip penetration as a function of tunneling voltage has been reported previously for organic materials. To our knowledge, however, no attempt was made to determine electronic levels from those measurements, see for instance: F. G. C. Hogenraad, A. C. R. Hogervorst, P. M. L. O. Scholte, and F. Tunistra, *Ultramicroscopy* **42–44**, 1004 (1992); W. Mizutani, M. Shigeno, Y. Sakakibara, K. Kajimura, M. Ono, S. Tanishima, K. Ohno, and N. Toshima, *J. Vac. Sci. Technol. A* **8**, 675 (1990).
[30] M. Brinkmann, G. Gadret, M. Muccini, C. Taliani, N. Masciocchi, and A. Sironi, *J. Am. Chem. Soc.* **122**, 5147-5157 (2000).
[31] H. B. Michaelson, *J. Appl. Phys.* **48**, 4729 (1977).
[32] C. Hosokawa, H. Higashi, H. Nakamura, and T. Kusumoto, *Appl. Phys. Lett.* **67**, 3853 (1995).
[33] M. Matsumura and T. Akai, *Jpn. J. Appl. Phys.* **35**, 5357 (1996).
[34] M. Probst and R. Haight, *Appl. Phys. Lett.* **71**, 202 (1997).
[35] A. Schmidt, M. L. Anderson, and N. R. Armstrong, *J. Appl. Phys.* **78**, 5619 (1995).
[36] S. T. Lee, Y. M. Wang, X. Y. Hou, and C. W. Tang, *Appl. Phys. Lett.* **74**, 670 (1999).
[37] E. M. Conwell, *Synth. Metals* **83**, 101 (1996).
[38] A. Curioni and W. Andreoni, in preparation.
[39] A. Curioni, M. Boero, and W. Andreoni, *Chem. Phys. Lett.* **294**, 263, (1998).
[40] P. E. Burrows, Z. Shen, V. Buloic, D. M. McCarty, S. Forrest, J. A. Cronin, and M. E. Thompson, *J. Appl. Phys.* **79**, 7991 (1996).
[41] H. Riel, Diplomarbeit, Institut für Technische Physik I, Friedrich-Alexander Universität, Erlangen-Nürenburg, Germany (April 1998).
[42] L. Rossi, P. Müller, S. F. Alvarado, and W. Rieß, *Proc. E-MRS*, Strasbourg, France, May 30 - June 2, 2000 (to be published in Synthetic Metals).
[43] G. Parthasarathy, P. E. Burrouws, V. Kalfin, V. G. Kozlov, and S. R. Forrest, *Appl. Phys. Lett.* **72**, 2138 (1998).
[44] P. M. Borsenberger and D. S. Weiss, *Organic Photo Receptors for Imaging Systems*, Marcel Dekker, Inc., New York, Basel, Hong Kong, 1993 and references therein.
[45] R. G. Kepler, P. M. Beeson, S. J. Jacobs, R. A. Anderson, M. B. Sinclair, V. S. Valencia, and P. A. Cahill, *Appl. Phys. Lett.* **66**, 3618 (1995); T. Tsutsui, H. Tokuhisa, and M. Era, *Proc. SPIE* Vol. 3281, 230 (1998).
[46] A. G. Mückl, S. Berleb, W. Brütting, and M. Schwoerer, *Proc. 2nd Int'l Conf. on Electroluminescence of Molecular Materials and Related Phenomena, ICEL-2*, Sheffield, UK, May 13-15, 1999 (to be published in Synthetic Metals).
[47] I. I. Smolyaninov and M. S. Khaikin, *Physics Lett. A* **149**, 410 (1990); I. I. Smolyaninov, *Surf. Sci.* **364**, 135 (1996).
[48] E. Flaxer, O. Sneh, and O. Chesnovski, *Science* **262**, 2012 (1993).
[49] D. G. Lidzey, S. F. Alvarado, P. F. Seidler, A. Bleyer, and D. D. C. Bradley, *Appl. Phys. Lett.* **71**, 2008 (1997).
[50] D. G. Lidzey, D. D. C. Bradley, S. F. Alvarado, and P. F. Seidler, *Nature* **386**, 135 (1997).
[51] J. V. Barth, H. Burne, G. Ertl, and R. J. Behm, *Phys. Rev. B* **42**, 9307 (1990).
[52] R. Berndt and J. K. Gimzewski, *Phys. Rev. Lett.* **67**, 3796 (1991) and references therein.
[53] Y. Sato, S. Ichinosawa, and H. Kanai, *Inorganic and Organic Electroluminescence*, R. H. Mauch and H.-L. Gummlich, Eds., Wissenschaft und Technik, Berlin, 1996.

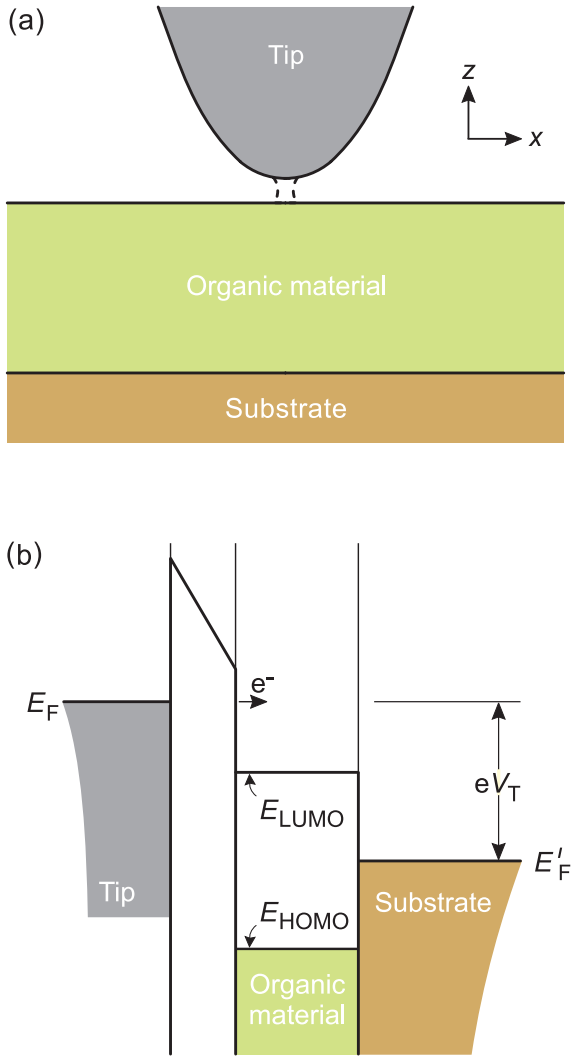

FIG. 1. (a) Geometry and (b) energy diagram for a typical STM configuration, where charge injection into the organic material occurs via tunneling through a vacuum barrier.

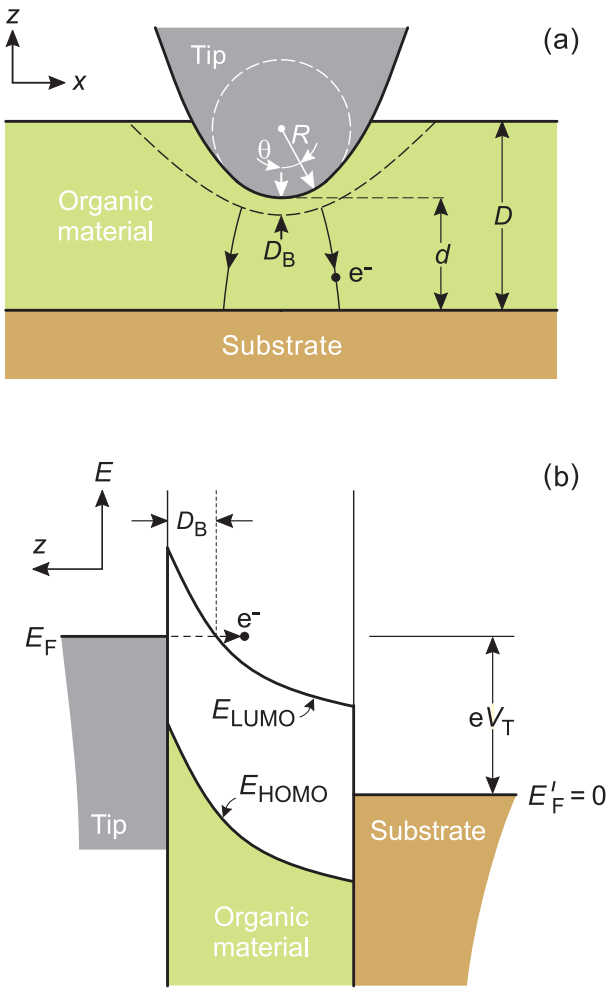

FIG. 2. (a) Geometry and (b) energy diagram for tunneling in the point contact case. Injection into the organic material occurs via tunneling through a Schottky barrier of thickness D_B. (Image force contributions not shown.)

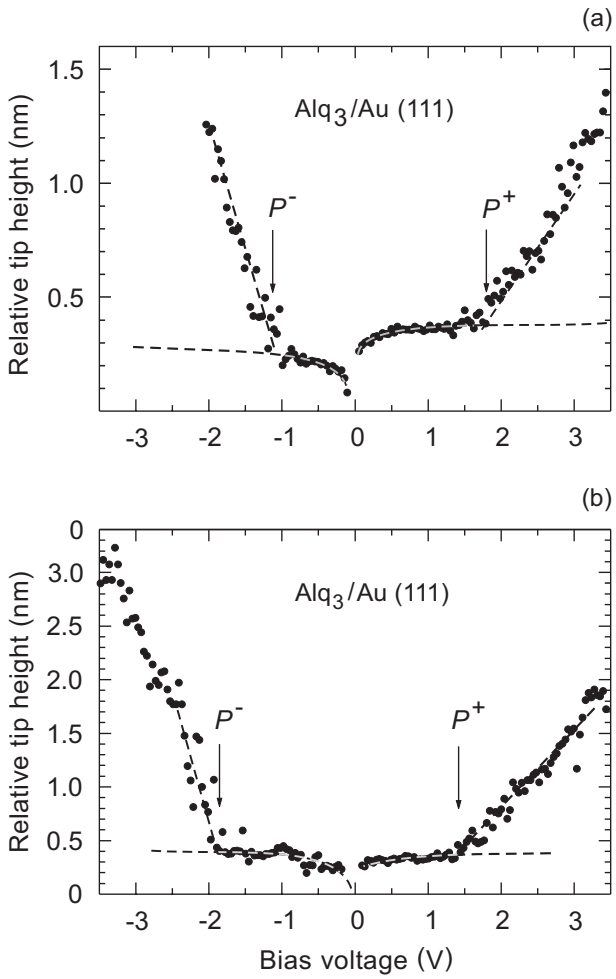

FIG. 3. z–V curves collected on an Alq_3 thin film deposited on a Au(111) substrate. The dashed curve represents the typical tip displacement measured for the clean Au(111) substrate. Curves a and b were collected at different locations of the sample. The threshold for injection of charge carriers into electron (P^-) and hole polaron (P^+) states is marked by a sharp decrease of the slope of the z–V curve. The shift in charge injection thresholds in panels (a) and (b), is discussed in the text.

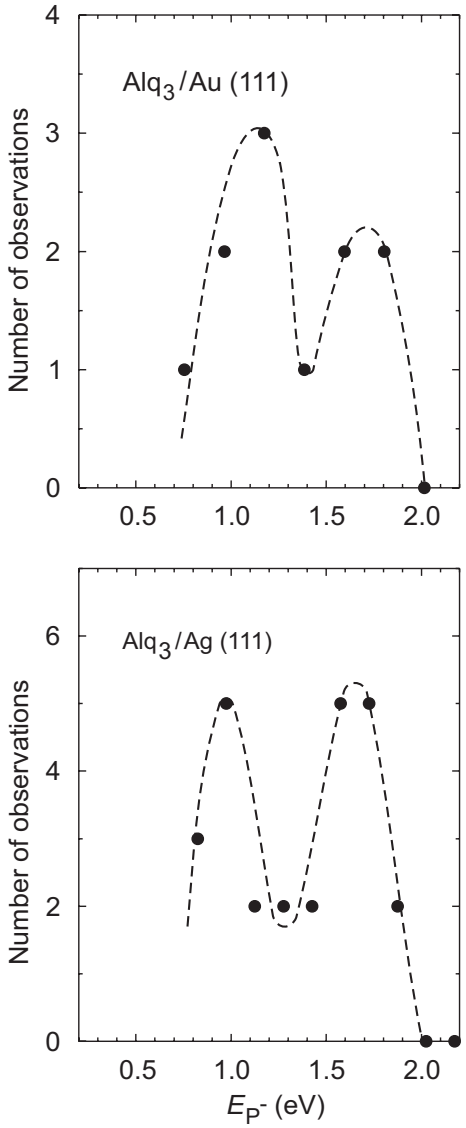

FIG. 4. Histograms of the injection threshold of electrons into an Alq_3 thin film deposited on a Au(111) and a Ag(111) substrate. The dashed lines are guides to the eye.

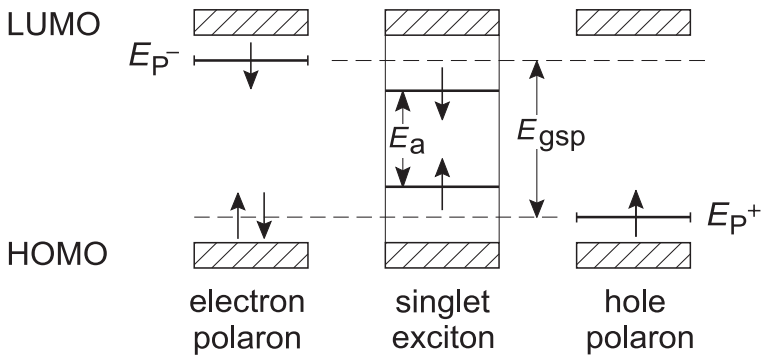

FIG. 5. Diagram illustrating the definition used to determine the exciton binding energy, E_b. The parameter E_{gsp} is the single-particle band gap, determined from z–V curves, see Figure 3; E_a is the optical absorption threshold.

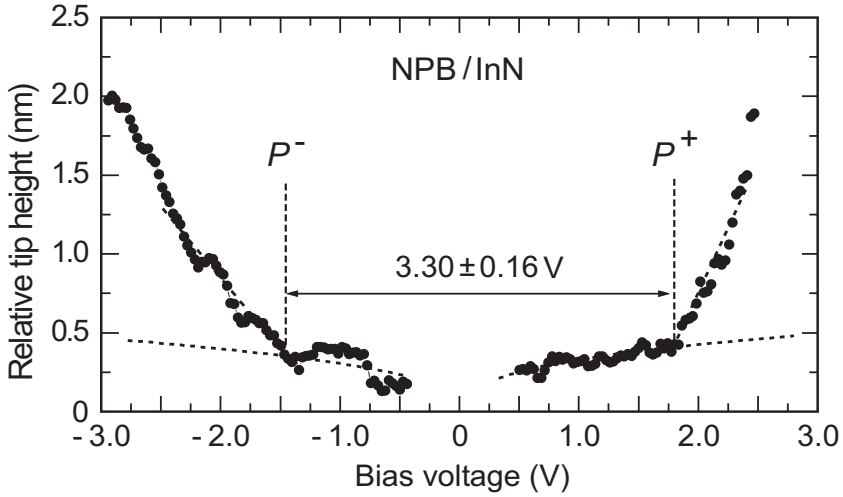

FIG. 6. z–V curves collected on an NPB thin film deposited on an InN substrate.

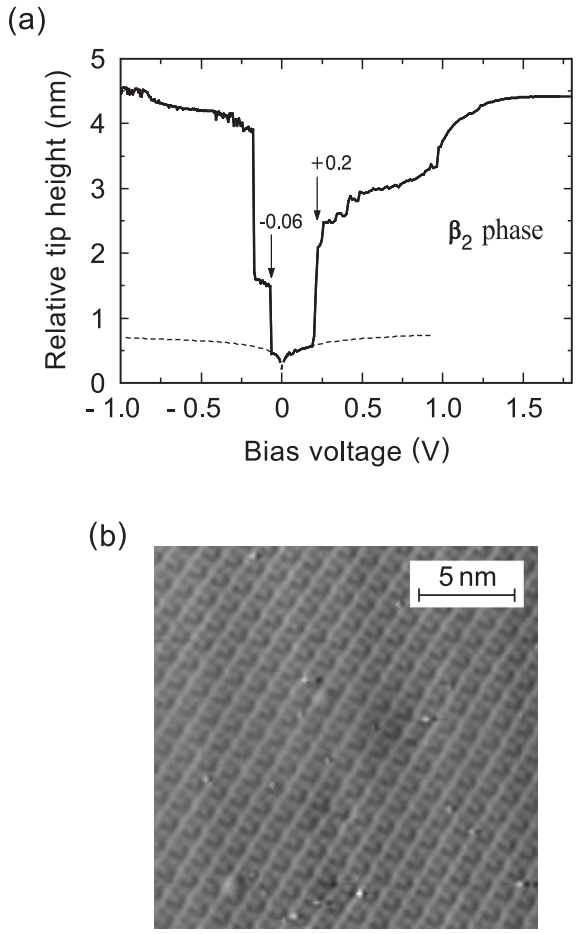

FIG. 7. (a) z–V curves collected on a CuPc thin film deposited on a Au(111) substrate. The difference between the z–V curves of the CuPc sample (solid line) and the clean substrate (dashed line), at high bias voltages is an approximate measure of the thickness of the CuPc layer. (b) Typical in-plane crystal structure of the CuPc crystallites on which this measurement was made.

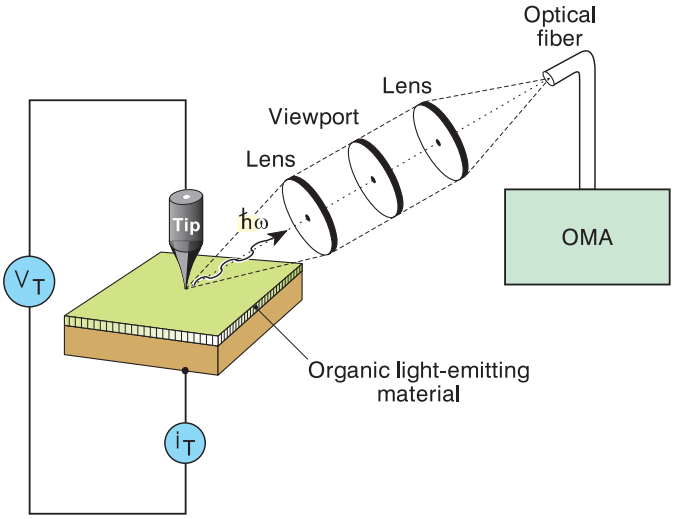

FIG. 8. Schematics of the STM-excited electroluminescence setup. For wavelength-integrated intensity measurements the optical fiber and optical multichannel analyzer (OMA) are replaced by an avalanche photodiode.

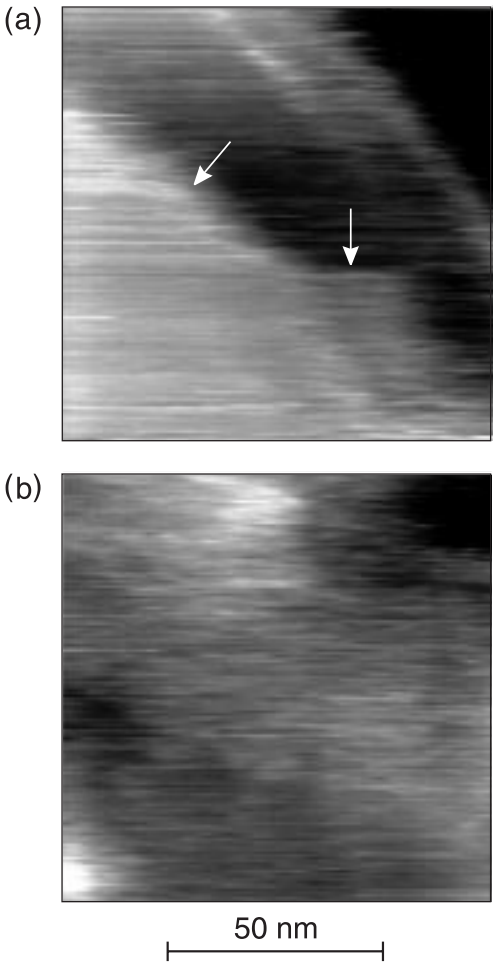

FIG. 9. STM topographs of an Alq_3-coated Au(111) surface showing (a) smooth terraces and (b) a region exhibiting a higher degree of roughness. The arrows in panel (a) indicate molecular steps.

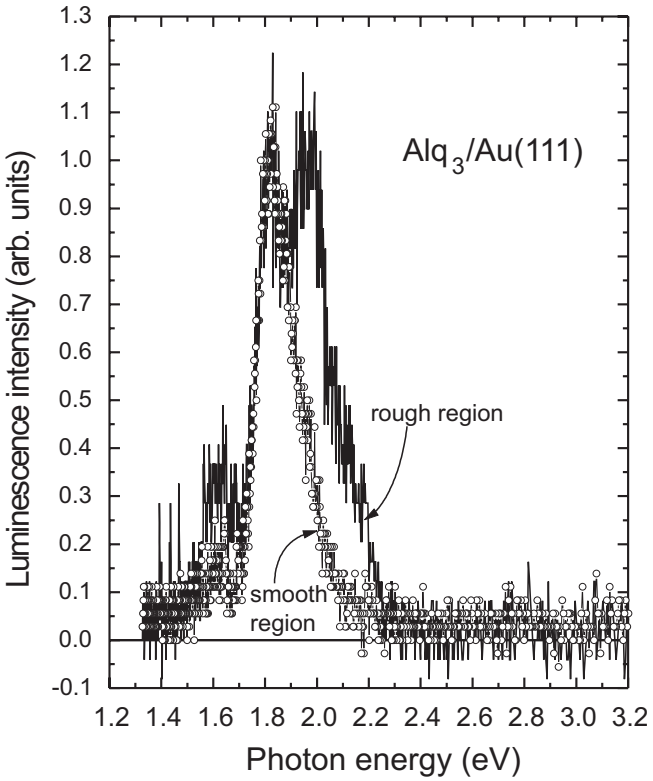

FIG. 10. STM-excited electroluminescence spectra collected on a flat terrace and a region of high corrugation, of the sample in Figure 9(a) and (b) respectively, at a tip bias of -4.5 V and a tunneling current of 200 pA.

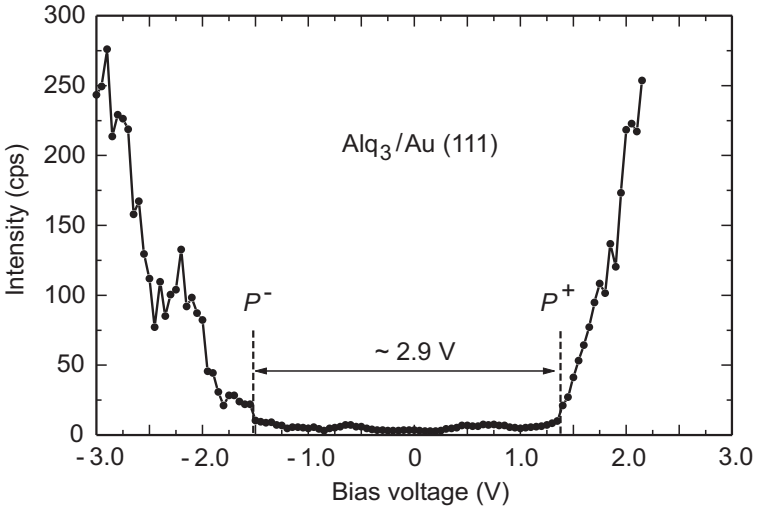

FIG. 11. Typical wavelength-integrated STL intensity, I_{L}, versus V_{T} curve collected at a tunneling current of $i_{\mathrm{T}} = 150$ pA on an Alq_3 thin film deposited on Au(111).